Robust Electrocatalytic Nitrate-to-N_2 Conversion Enabled by Engineered Bi_2O_3-Cu_2O Heterojunction on Cu foam under High-Salinity and Wide-pH Conditions

Shuwei Gu,[†a] Ziyan Zhang,[†a] Xinyu Deng,[a] Jue Wu,[b] Jiale Wang,[a] Jing Wang,[a] Xin Jin,[a] Hui Xu,[a] Ding Wang,[a] Guisheng Li,[a] and Huan Shang[a]*

[a]School of Materials and Chemistry, University of Shanghai for Science and Technology, Shanghai 200093, P. R. China.

[b]Department of Mathematics and Science, Fujian Jiangxia University, Fuzhou, 350108, China.

*Corresponding authors: huanshang1992@163.com.

1. Experimental section.

1.1. Chemicals and Materials. CH_3OH, CH_3CH_2OH, Cu Foam, C_3H_6O, $Bi(NO_3)_3 \cdot 5H_2O$. All analytical-grade chemicals and materials are purchased from a commercial company and can be used without further purification.

1.2. Prepare OV@CF heterojunction. Firstly, the purchased CuF was ultrasonically cleaned with acetone, ethanol and water for 15 minutes. Then, it was cut into a size of 1 cm×1.5 cm. The overall CuF electrode was pre-treated in a reducing atmosphere (Ar) at a heating rate of 5 °C min^{-1} for 3 hours at 400°C to generate oxygen vacancies (OVs) on the electrode surface.[1]

1.3. Prepare Bi-Cu@CF heterojunction. The purchased CuF was ultrasonically cleaned with acetone, ethanol and water for 15 minutes. Then, it was cut into a size of 1 cm×1.5 cm. The overall CuF electrode was pre-treated in a reducing atmosphere (Ar) at a heating rate of 5 °C min^{-1} for 3 hours at 400°C to generate oxygen vacancies (OVs) on the electrode surface. Then, a uniform layer of acetone solution with a Bi concentration of 4 mg/mL was deposited on the fabricated CuF(OV) integrated electrode. During the deposition process, it was carried out under the illumination of an infrared lamp, which accelerated the evaporation of the solvent and prevented the formation of solvent accumulation due to surface tension. Finally, the Bi_2O_3/Cu_2O-OV@CF electrode was obtained again by treating the Bi-deposited electrode at 400°C in a reducing atmosphere (Ar) at a heating rate of 5°C min^{-1} for 3 hours.

2.Characterization Method

2.1 Physical Characterization. The surface morphology and elemental distribution of the catalysts were examined using field-emission scanning electron microscopy (FESEM, ZEISS Merlin Compact, Germany) and transmission electron microscopy (TEM, JEOL JEM-2100, Japan) equipped with an energy-dispersive X-ray spectrometer (EDS). High-resolution TEM (HRTEM) images were acquired on a Thermo Scientific Talos F200X microscope operated at an accelerating voltage of 200 kV. The crystalline structures of the samples were characterized by X-ray diffraction (XRD, Bruker D8 Advance) using Cu Kα radiation under operating conditions of 40

kV and 30 mA, with a scanning rate of 5°·min^{-1}. Raman spectra were collected on a HORIBA LabRAM HR Evolution spectrometer using a 532 nm Ar^+ laser as the excitation source. The surface chemical states of the samples were analyzed by X-ray photoelectron spectroscopy (XPS, Thermo Scientific K-Alpha) equipped with a monochromatic Al Kα radiation source (200 W). Ultraviolet–visible diffuse reflectance spectroscopy (UV-vis DRS, Shimadzu UV-2600) was employed to investigate the optical absorption properties of the samples. Electron paramagnetic resonance (EPR, Bruker EMX Nano) spectroscopy was performed to detect oxygen vacancies (OVs), chloride species (Cl^-), and hydrogen radicals (•H). 5,5-Dimethyl-1-pyrroline N-oxide (DMPO) was used as a spin-trapping agent for •H. After electrolysis at a current density of 5 mA·cm^{-2} for 5 min, the electrolyte was mixed with DMPO and transferred into a quartz tube for EPR measurements.

2.2 Electrochemical Measurements. Electrochemical measurements were conducted on a CHI 660D electrochemical workstation (CH Instruments, Shanghai) using an undivided three-electrode configuration. A platinum plate and a saturated calomel electrode (SCE) were used as the counter and reference electrodes, respectively. The prepared Bi-Cu@CF electrode (geometric area: 1 cm × 1 cm) served as the working electrode. The electrolyte consisted of a mixed solution of 0.1 M K_2SO_4 and 0.04 M KCl. For each experiment, 50 mL of electrolyte containing 50 mg·L^{-1} NO_3^--N was added to the electrochemical cell. Prior to testing, the electrolyte was purged with high-purity argon (99.999%) for at least 30 min to remove dissolved oxygen.Linear sweep voltammetry (LSV) was performed to evaluate the nitrate reduction reaction (NO_3RR) at a scan rate of 5 mV·s^{-1}. Electrochemical impedance spectroscopy (EIS) measurements were carried out over a frequency range from 100 kHz to 0.01 Hz with an AC amplitude of 5 mV. The electrochemical double-layer capacitance (C_{dl}) was estimated from cyclic voltammetry (CV) tests conducted at different scan rates within the non-faradaic potential region (−0.21 to −0.09 V vs. SCE). The capacitive current density was calculated at −0.15 V using $\Delta j = (j_a - j_c)/2$. Chronoamperometry (i-t) tests were employed to evaluate the stability and current response of the electrode.

Furthermore, the NO_3RR electrocatalytic performance of the Bi-Cu@CF cathode was systematically investigated under various applied potentials (−1.1, −1.2, −1.3, −1.4, and −1.5 V vs. SCE), different Cl^- concentrations, and different initial NO_3^--N concentrations (10, 20, 50, 100, and 500 $mg \cdot L^{-1}$). The solution pH was adjusted using HCl or KOH as required.

2.3 In Situ Fourier Transform Infrared (*In situ* FTIR) Spectroscopy. In situ FTIR measurements were carried out using an iS50 Fourier transform infrared spectrometer. To prepare the working electrode, 2.0 mg of Bi-Cu@CF catalyst was dispersed in a mixed solvent containing 200 μL ethanol and 400 μL deionized water, followed by the addition of 10 μL Nafion solution. The mixture was ultrasonicated for 1 h to obtain a homogeneous catalyst ink. Subsequently, 600 μL of the ink was drop-cast onto carbon paper and dried naturally to serve as the working electrode.A platinum plate and a saturated calomel electrode were used as the counter and reference electrodes, respectively. The electrolyte consisted of a mixed solution of 0.1 M K_2SO_4 and 0.04 M KCl containing 50 ppm NO_3^--N. A background spectrum was recorded at open-circuit potential, followed by continuous collection of *in situ* FTIR spectra every 100 s at an applied potential of −0.7 V (vs. SCE).

3. Product analysis.

3.1 Determination of nitrate-N (NO_3^--N). The electrolyte solution was collected and filtered through a 22 μm aqueous-phase membrane, then quantitatively diluted to 5 mL with deionized water (within the detection range). Subsequently, 200 μL of 1 M HCl and 20 μL of sulfamic acid solution (0.8% w/v) were sequentially added to the diluted solution. After standing for 5 minutes, the UV-Vis absorption spectrum was measured, and the absorption intensities at 220 nm and 275 nm were recorded. The concentration of NO_3^--N was calculated by the absorbance value A (A=A220 nm-2A275 nm). The potassium nitrate crystal was dried at 105-110 ℃ for 2 h in advance.

3.2 Determination of nitrite-N (NO_2^--N). A color reagent was prepared by mixing 4 g of p-aminobenzenesulfonamide, 0.2 g of N-(1-Naphthyl) ethylenediamine

dihydrochloride, 50 mL of ultrapure water, and 10 mL of phosphoric acid (ρ = 1.70 g/mL), followed by dilution to a final volume of 100 mL.[2] An aliquot of the electrolyte solution was collected, filtered through a 0.22 μm aqueous-phase membrane, and quantitatively diluted to 5 mL with deionized water (within the detection range). Subsequently, 0.1 mL of the color reagent was added to the diluted solution, mixed thoroughly, and allowed to stand for 20 min. The absorption intensity at 540 nm was recorded.

3.3 Determination of NH_4^+-N. Ammonia-N was determined using Nessler's reagent as the color agent. An aliquot of the electrolyte solution was filtered through a 0.22 μm aqueous-phase membrane filter and quantitatively diluted to 5 mL with deionized water (within the detection range). Subsequently, 0.1 mL of potassium sodium tartrate solution and 0.1 mL of Nessler's reagent were sequentially added to the diluted solution. After thorough mixing and standing for 15 min, the UV-Vis absorption spectrum was measured, and the absorption intensity at 420 nm was recorded. A concentration-absorbance calibration curve was established using a series of standard ammonium chloride solutions and the ammonium chloride crystal was dried at 100℃ for 2 h in advance. The potassium sodium tartrate solution was prepared by dissolving 50 g of potassium sodium tartrate tetrahydrate ($KNaC_4H_4O_6 \cdot 4H_2O$) in 100 mL of ultrapure water, heated to boiling to remove residual ammonium ions, cooled to room temperature, and diluted to a final volume of 100 mL.

4. Calculation of nitrate conversion and product selectivity.

The conversion of NO_3^- was calculated as equation 1:

$$C(NO_3^-)\% = \frac{C_0(NO_3^- - N) - C_t(NO_3^- - N)}{C_0(NO_3^- - N)} \times 100\% \quad (1)$$

The selectivity of the product was calculated as equation 2:

$$S(N_2)\% = \frac{C_0(NO_3^- - N) - C_r(NO_2^- - N) - C_t(NH_4^+ - N)}{\Delta C(NO_3^- - N)} \times 100\% \quad (2)$$

Where C_0 (NO_3^-) (mg L^{-1}) and C_t (NO_3^-) (mg L^{-1}) are the initial nitrate (NO_3^--N) concentration and nitrate concentration after different electrocatalytic reduction time,

respectively. C_t (NO_2^--N) and C_t (NH_4^+-N) represent the concentrations of nitrite and ammoniums.

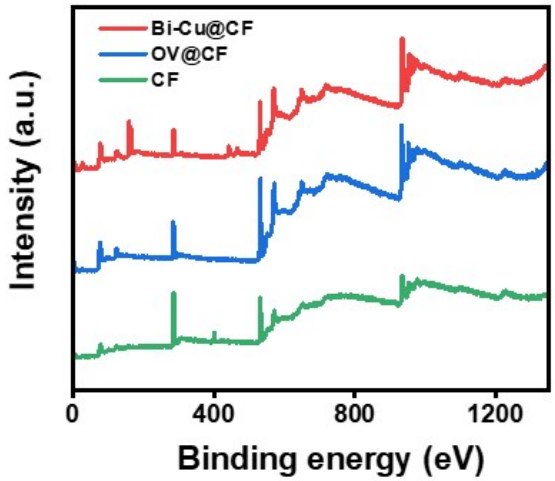

Fig. S1. XPS survey spectrum of Bi_2O_3-Cu_2O/Cu Foam, Cu_2O/Cu Foam, and Cu Foam.

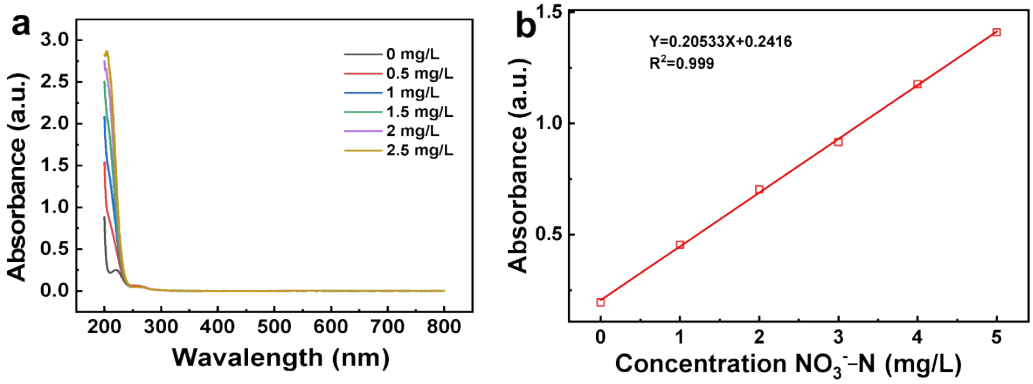

Fig. S2. Standard curve of NO_3^--N. (a) UV-vis absorption spectra of various concentration gradients of NO_3^--N. (b) The concentration-absorbance calibration curves of NO_3^--N.

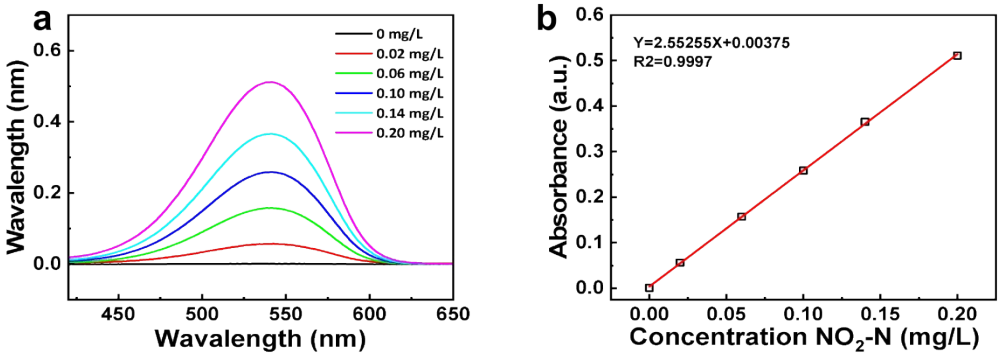

Fig. S3. Standard curve of NO_2^--N. (a) UV-vis absorption spectra of various concentration gradients of NO_2^--N. (b) The concentration-absorbance calibration curves of NO_2^--N.

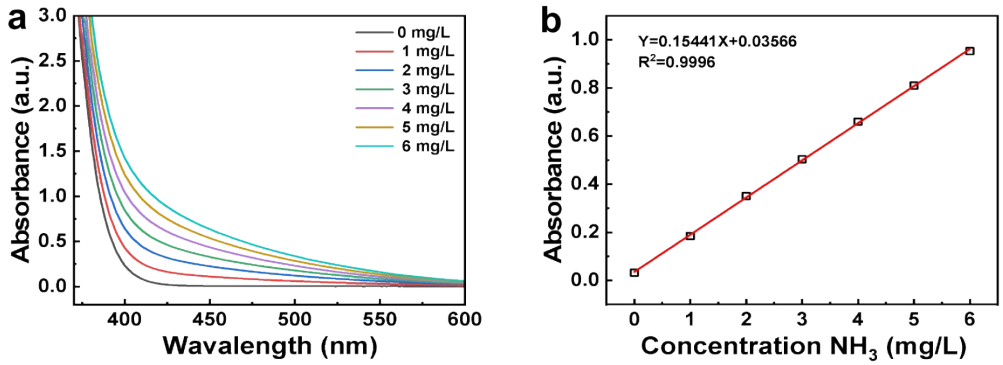

Fig. S4. Standard curve of NH_4^+-N. (a) UV-vis absorption spectra of various concentration gradients of NH_4^+-N. (b) The concentration-absorbance calibration curves of NH_4^+-N.

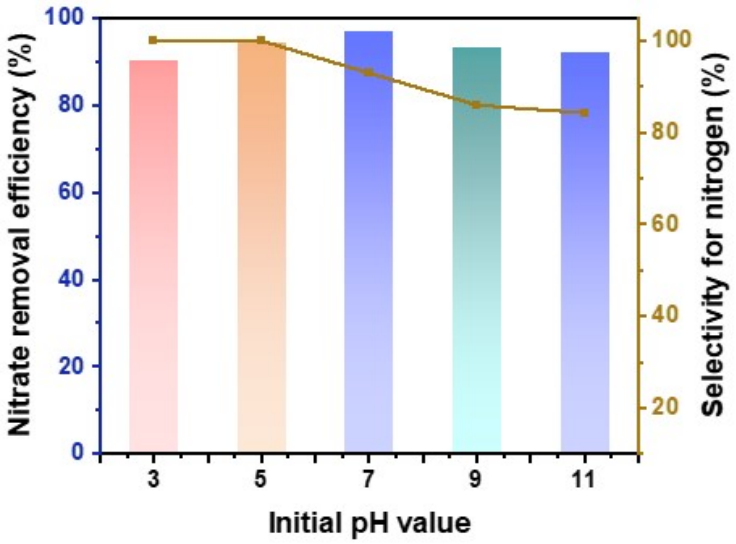

Fig. S5. The effects of different pH values. pH values represent the pH value of the electrolyte after debugging. Adjust the acidity and alkalinity using sulfuric acid and sodium hydroxide.

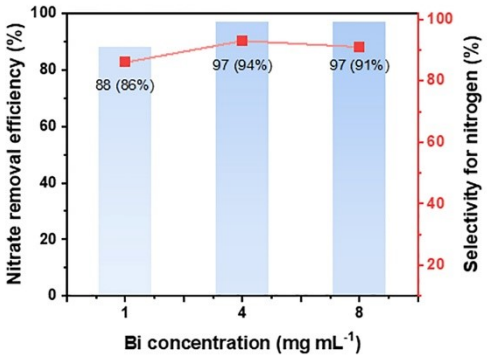

Fig. S6. The influence of B_2O_3 content on the performance of electrocatalytic reduction of nitrate.

A Bi concentration of 4 mg/mL exhibits an optimal balance, maximizing both the nitrate efficiency removal of 97% and the conversion towards the benign N_2 with selectivity of 94%. The best Bi_2O_3-Cu_2O heterojunction electrode in this study is selected with this concentration of 4 mg/mL.

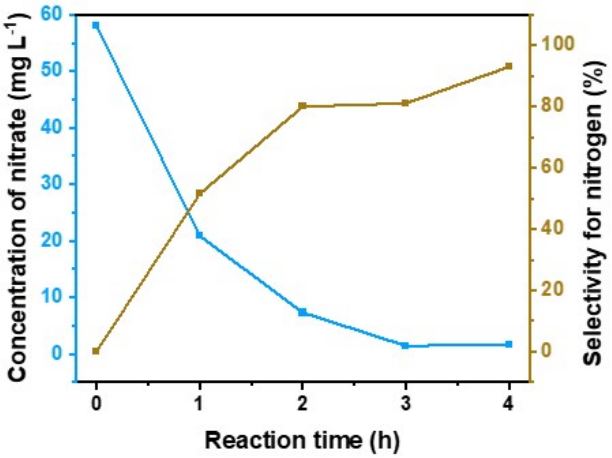

Fig. S7. Nitrate removal efficiency and selectivity for N_2 during the electrocatalytic nitrate reduction reaction by Bi-Cu@CF.

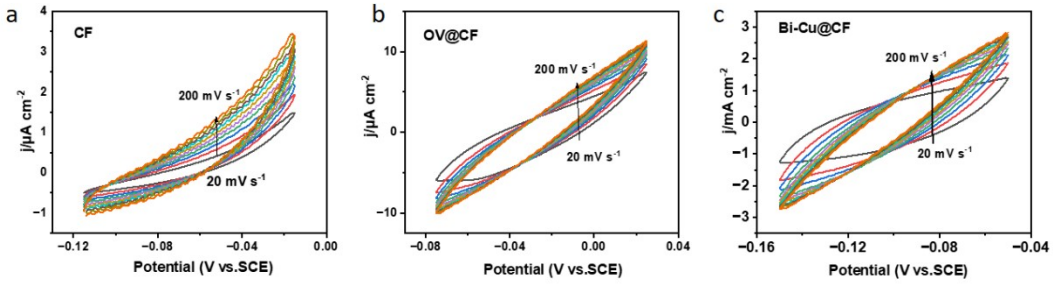

Fig. S8. CV curves of Bi-Cu@CF, OV@CF, CF.

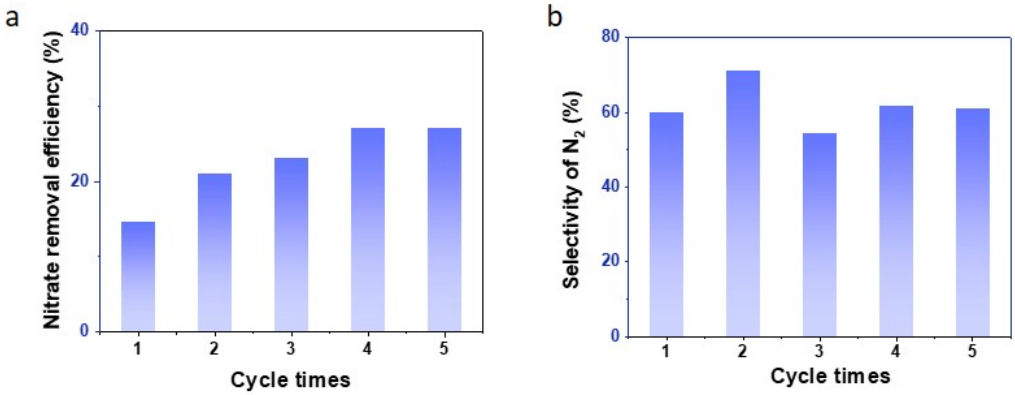

Fig. S9. (a) Nitrate removal efficiency and (b) selectivity for N_2 in simulated wastewater using the electrocatalytic nitrate reduction reaction by Bi-Cu@CF.

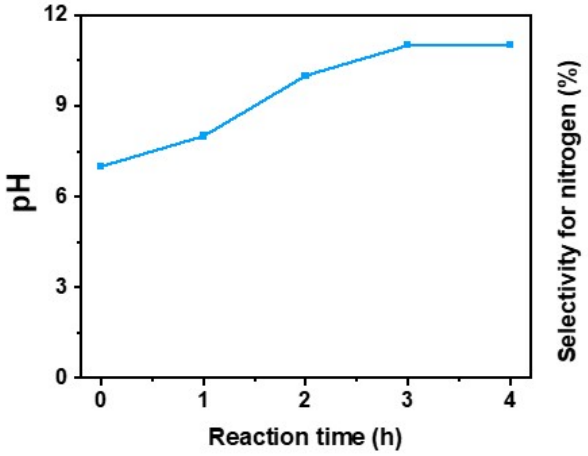

Fig. S10. pH changes during the electrocatalytic nitrate reduction reaction by Bi-Cu@CF.

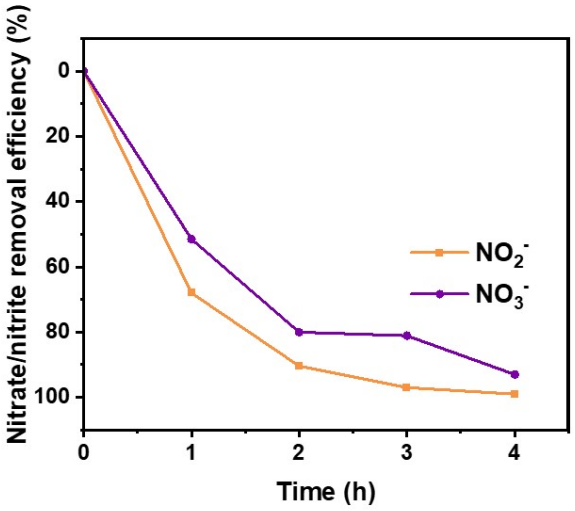

Fig. S11. Comparison of nitrate (NO_3^-) and nitrite (NO_2^-) as substrates to identify the rate-determining step during the electrocatalytic reduction reaction by Bi-Cu@CF.

Table S1. The types and concentrations of various coexisting substances in the simulated wastewater.[3]

Substance	Concentration
$NaHCO_3$	5 mmol L^{-1}
$CaCl_2$	2 mmol L^{-1}
$MgSO_4$	0.3 mmol L^{-1}
KCl	0.2 mmol L^{-1}
NO_3^--N	50 mg L^{-1}

Notes: $C_2O_4^{2-}$ represents organic acids commonly present in industrial wastewater, which can compete for active sites or act as sacrificial agents. PO_4^{3-} is known for its high affinity for surface adsorption, allowing us to test competitive adsorption against nitrate on the catalyst surface. $S_2O_8^{2-}$ is a strong oxidizing agent sometimes present in advanced oxidation processes; it tests the stability and selectivity of our catalyst under potentially oxidative conditions. This combination allows us to evaluate the robustness of the Bi_2O_3-Cu_2O heterojunction electrode against a range of realistic anionic

interferences that could affect nitrate reduction efficiency and N_2 selectivity.

Table S2. Comparison of eNO_3RR performances with reported catalysts.[4-8]

Catalysts	NO_3^--N (mg·L-1)	NO_3^--N Removal (%)	N_2 Selectivity (%)	Ref.
Bi-Cu@CF	50	97	94	This work
2D-MXene membrane	10	73	82.8	[4]
Co_3O_4-TiO_2/Ti	50	89	30	[5]
Fe@Gnc	100	50	80	[6]
FeCo-NPCNFs	100	78.5	85	[7]
CuNi	100	95	65	[8]

References

[1] J. Dai, Y. Tong, L. Zhao, Z. Hu, C.-T. Chen, C.-Y. Kuo, G. Zhan, J. Wang, X. Zou, Q. Zheng, W. Hou, R. Wang, K. Wang, R. Zhao, X.-K. Gu, Y. Yao, L. Zhang, Spin polarized Fe_1−Ti pairs for highly efficient electroreduction nitrate to ammonia, Nature Communications, 15 (2024) 88.

[2] Y. Dai, S. Li, X. Li, K. Liu, Y. Guo, H. Li, B. Jiang, Tandem Active Sites in Cu/Mo-WO_3 Electrocatalysts for Efficient Electrocatalytic Nitrate Reduction to Ammonia, Advanced Functional Materials, 35 (2025) 3263-3275.

[3] X. Chen, T. Zhang, M. Kan, D. Song, J. Jia, Y. Zhao, X. Qian, Binderless and Oxygen Vacancies Rich FeNi/Graphitized Mesoporous Carbon/NiFoam for Electrocatalytic Reduction of Nitrate, Environmental Science & Technology, 54 (2020) 13344-13353.

[4] Y. Li, J. Ma, T.D. Waite, M.R. Hoffmann, Z. Wang, Development of a Mechanically Flexible 2D-MXene Membrane Cathode for Selective Electrochemical Reduction of Nitrate to N_2: Mechanisms and Implications, Environmental Science & Technology, 55 (2021) 10695-10703.

[5] L. Su, K. Li, H. Zhang, M. Fan, D. Ying, T. Sun, Y. Wang, J. Jia, Electrochemical nitrate reduction by using a novel Co_3O_4 /Ti cathode, Water Research, 120 (2017) 1-11.

[6] K. Fan, W. Xie, J. Li, Y. Sun, P. Xu, Y. Tang, Z. Li, M. Shao, Active hydrogen boosts electrochemical nitrate reduction to ammonia, Nature Communications, 13 (2022) 7958.

[7] H. Luo, S. Li, Z. Wu, M. Jiang, M. Kuang, Y. Liu, W. Luo, D. Zhang, J. Yang, Relay Catalysis of Fe and Co with Multi-Active Sites for Specialized Division of Labor in Electrocatalytic Nitrate Reduction Reaction, Advanced Functional Materials, 34 (2024) 2403838.

[8] Y. Zhang, Y. Zhao, Z. Chen, L. Wang, P. Wu, F. Wang, Electrochemical reduction of nitrate via Cu/Ni composite cathode paired with Ir-Ru/Ti anode: High efficiency and N_2 selectivity, Electrochimica Acta, 291 (2018) 151-160.